



THE UNIVERSITY *of* EDINBURGH

Edinburgh Research Explorer

Experimental optimisation of power for large arrays of cross-flow tidal turbines

Citation for published version:

Sutherland, D, Ordonez-Sanchez, S, Belmont, M, Moon, I, Steynor, J, Davey, T & Bruce, T 2018, 'Experimental optimisation of power for large arrays of cross-flow tidal turbines', *Renewable Energy*, vol. 116, no. Part A, pp. 685-696. <https://doi.org/10.1016/j.renene.2017.10.011>

Digital Object Identifier (DOI):

[10.1016/j.renene.2017.10.011](https://doi.org/10.1016/j.renene.2017.10.011)

Link:

[Link to publication record in Edinburgh Research Explorer](#)

Document Version:

Peer reviewed version

Published In:

Renewable Energy

General rights

Copyright for the publications made accessible via the Edinburgh Research Explorer is retained by the author(s) and / or other copyright owners and it is a condition of accessing these publications that users recognise and abide by the legal requirements associated with these rights.

Take down policy

The University of Edinburgh has made every reasonable effort to ensure that Edinburgh Research Explorer content complies with UK legislation. If you believe that the public display of this file breaches copyright please contact openaccess@ed.ac.uk providing details, and we will remove access to the work immediately and investigate your claim.



Experimental Optimisation of Power for Large Arrays of Cross-Flow Tidal Turbines

Duncan Sutherland^{a,*}, Stephanie Ordonez-Sanchez^b, Michael R. Belmont^c,
Ian Moon^c, Jeffrey Steynor^d, Thomas Davey^d, Tom Bruce^a

^a*Institute for Energy Systems, School of Engineering, University of Edinburgh*

^b*Energy Systems Research Unit, University of Strathclyde*

^c*College of Engineering, Mathematics and Physical Sciences, University of Exeter,
University of Exeter*

^d*FloWave Ocean Energy Research Facility, University of Edinburgh*

Abstract

As commercial scale tidal energy devices are shortly to be deployed in the first arrays, the knowledge of how different array layouts perform is a key and under-examined field. Here, the Momentum Reversal Lift (MRL) turbine, developed by the University of Exeter, is deployed in five different array layouts utilising up to 15 devices. The use of dynamic turbines allows the inclusion of analysis of the effects of flow direction in the wake.

The layouts investigated explore the effect of lateral and stream-wise turbine spacings as well as differences between staggered and in-line layouts on power. The staggered array with decreased streamwise spacing is shown to have the highest total power per ‘footprint’ area among the layouts tested. For the staggered arrays, increased downstream separation had little effect on total power generated, while decreasing the lateral spacing below 2 rotor diameters decreased the power. The in-line arrays showed a lower power per device but similar total power. It was also shown that increased in-

*d.sutherland@ed.ac.uk
Preprint submitted to Renewable Energy August 19, 2017
URL: www.eng.ed.ac.uk/research/institutes/ies (Duncan Sutherland),
www.strath.ac.uk/esru/research/hydrowavetidalpower/ (Stephanie Ordonez-Sanchez), emps.exeter.ac.uk/engineering/research/cws (Michael R. Belmont), www.flowavett.co.uk/ (Thomas Davey)

flow into a turbine didn't necessarily lead to an increased power extraction. The decrease in power with a decrease in streamwise spacing is in-line with theoretical and CFD predictions.

Keywords: Renewables, Tidal Energy, Arrays, Scale Testing, Wake Interactions, Physical Modelling

1. Introduction

Tidal energy is considered a potentially significant contributor to the UK's energy mix, with estimates ranging from 15.7 TWh/year [1] and 20.6 TWh/year [2] which would account for 4.6% to 6.1% of the UK's electricity requirements [3]. With several commercial scale prototypes tested in isolation, the focus of the hydrodynamic research has shifted towards both second generation technologies optimised for specific environments and the interaction of devices in arrays. This work focuses on the novel Momentum Reversal Lift (MRL) turbine designed by the University of Exeter in conjunction with Aquascientific Ltd, using up to 15 scale models in a variety of array configurations to assess the effect of layout and spacing on power output. The optimum spacing for turbines is critical to extract maximum power and to predict loadings in arrays and is a field which has had limited experimental testing given the stage of commercial array projects. This work builds upon the work by: Janssen and Belmont [4] and Ordonez *et al.* [5] assessing the extractable power and wake evolution in both an individual turbine and a four turbine array, as well as CFD work on both device and array optimisation [6, 7, 8, 9].

49 2. Background

50 2.1. Tidal Turbine Arrays

51 Flow through an array of turbines is highly complex, due to the nature
52 of tidal energy sites [10, 11] and the interaction of turbine wakes [12, 13, 14].
53 Energy extraction devices in tidal channels can in theory utilise high global
54 blockage ratios, i.e. the ratio of total turbine swept area divided by the
55 channel cross-sectional area. By doing so they are in theory able to extract a
56 greater percentage of available power than in an open channel, increasing the
57 Lanchester-Betz ratio of 0.593 to 0.798 [15]. Staggering devices in rows use
58 upstream turbines, which provide local blockage, to accelerate flow between
59 them, so that the downstream turbines have a higher inflow velocity. The use
60 of these arrays has been theorised to increase extractable power for certain
61 downstream spacings [16]. To this end, several studies have focused on wake
62 evolution and downstream mixing [17, 12] with the goal of maximisation
63 of the local available power in the flow, which is expected to increase with
64 the cube of the flow speed. In addition, increasing the downstream spacing
65 between rows allows the wake after the first row to mix with the bypass and
66 free-stream flow to recover to a higher value, increasing the inflow to the
67 subsequent row. In principle it is possible that as a turbine causes bypass
68 flow acceleration around it, the downstream flow can be higher than the
69 upstream flow despite kinetic energy being extracted by the turbine, as the
70 total energy is conserved through a loss of head.

71 Local inflow velocity is not the only factor that will effect the extractable
72 power for a turbine. It is generally agreed that a more turbulent flow for the
73 equivalent velocity will induce less lift which in turn will reduce the power

74 that a turbine can extract. However, these effects are complex and depend
75 upon the scales of turbulence in question [18, 11]. Turbines are also sensitive
76 to flow direction which changes the effective angle of attack of the lifting
77 surfaces used as the prime mover to extract power. A theoretical exploration
78 of array layouts is given in Draper *et al.* [19].

79 Tank testing of tidal arrays to date has been limited, due in part to
80 the difficulty in finding appropriate testing facilities. Myers and Bahaj [20]
81 investigated array layouts through porous disks in a shallow tank with the
82 aim of maximising the flow acceleration through the array. Draper *et al.*
83 [17] conducted a similar study with the focus on the evolution of the wakes.
84 However, these studies investigated flow acceleration and not the extracted
85 power. Cooke *et al.* [21] used the thrust on the disk along with a near wake
86 velocity measurement to infer the power, finding power coefficients per disk
87 of ≈ 0.1 based on the global channel flow.

88 More complex flow effects caused by a dynamic turbine model (such as
89 rotational effects) are not present in porous disk experiments. Stallard *et al.*
90 [12] have investigated the layouts of up to ten three-bladed Horizontal Axis
91 Turbines (HATs), with lateral spacings of $1.5D$ and $2D$ (where D is a rotor
92 diameter) over two rows. They showed velocity deficits of 80% across the
93 turbines, $2D$ downstream by which point the wakes had begun merging and
94 were fully merged by $4D$. The widths of the individual wakes were seen to
95 expand to a maximum of $2D$ by $10D$ downstream. Power was measured via
96 a dynamometer but the variation of power with array layout is not reported
97 as the work focuses on the wake evolution.

98 Another HAT device study using two in-line three-bladed dynamic tur-

bine models at the deeper (2m) IFREMER tank was presented by Mycek *et al.* [22]. They showed a drop in turbine performance in the downstream device compared with a single turbine for a series of downstream spacings. They also show that in high turbulence environments, increased downstream mixing leads to lower velocity deficits increasing downstream device performance suggesting that velocity magnitude is more important than turbulence.

2.2. The Momentum Reversal Lift (MRL) turbine

The momentum reversal lift turbine, shown in Figure 1, was conceived by the University of Exeter and Aqua Scientific Ltd. This cross flow horizontal axis turbine has three symmetrical blades, each of which rotate through 180° for a full rotation of the shaft. The turbine is unique in that it utilises both lift and drag (momentum reversal) in order to generate rotational velocity in the prime mover. The turbine is designed primarily for shallow estuaries where the cross flow design will allow for high blockage ratios relative to a circular swept area device thus increasing power output. For a comprehensive overview of the turbine design see [4] and [7].

Initial experiments utilised both a balsa wood model in a wind tunnel and a metal turbine in a flume. These devices both showed promising maximum c_p values of ~ 0.5 , however these were in high blockage environments, 0.66 in the case of the flume [4]. The flume results were compared with a Immersed Body Force (IBF) CFD model utilising Large Eddy Simulation (LES), which showed good similarity with the experimental data, particularly for the lower torque range [6, 7].

The scale model turbines used here were previously tested in a wider flume at the IFREMER facility where some initial array configurations were

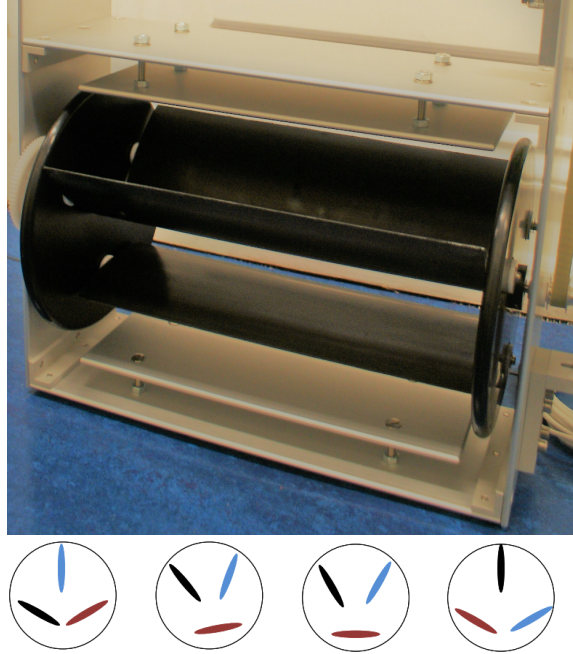


Figure 1: MRL turbine prototype used in the experiments described in this paper (top). The three bladed rotates around the shaft as it can be observed in the bottom figure. In the initial set up one blade is set completely flat while the others two start with a set angle.

Table 1: Array spacings in multiples of turbine diameters (D) and c_p of the centre turbine from CFD [8].

Downstream spacing	Lateral spacing	c_p
10D	3D	0.40
10D	6D	0.30
15D	3D	0.45
15D	6D	0.32

124 trialled [5]. The c_p values in a relatively open channel dropped to 0.14. In
125 these tests, the wake had not recovered to the upstream velocity magnitudes
126 by $20D$ downstream. In addition there was evidence of asymmetry in the
127 wake of a single turbine which is not evident in similar three bladed HAT
128 testing [12].

129 There have also been studies using the IBF model to investigate trends
130 in array layouts. These have investigated both changing spacings [8] and
131 varying resistive body force [9]. The former looked at a test matrix of two
132 lateral and two downstream turbine separations for three rows of turbines
133 in a 2-3-2 formation, with a blockage ratio of 0.044. Table 1 presents the
134 spacings and c_p values. It found the highest c_p values were in the narrower
135 (lateral) and longer (stream-wise) arrangement, with an increase in lateral
136 spacing causing a decrease in c_p . In addition, while it was found that the
137 blockage of the first row of turbines caused an acceleration into the middle
138 turbine in the second row, this did not necessarily mean an increase in c_p .

139 2.3. Aims and objectives of current study

140 A key goal in tidal energy research is to determine the extent to which
141 array layouts affect the extractable power. Arrays can be staggered or in-line
142 and the lateral and downstream spacings between devices can all be varied.

143 In this work five array layouts are trialled with the aim of maximising
144 power output and exploring the extent of the influences of spacing and lay-
145 out on both power and flow. The evolution of the wake is also investigated
146 through two sets of streamwise lines of velocity measurements, to allow com-
147 parison with previous studies. Array layouts are chosen to highlight the effect
148 of changing a single metric and to align with previous CFD modelling work.

149 3. Test Set-up and Methodology

150 3.1. Overview of the FloWave test tank

151 The array testing was conducted at the FloWave Test Tank facility. This
152 25 m diameter circular tank has the facility to provide combined wave and
153 current, with wavemakers located around the entire circumference. The nom-
154 inal test area has a diameter of 10 m. The tank is capable of generating
155 currents upwards of 1.6 ms^{-1} , using 28 drive units mounted in a plenum
156 chamber below the test floor. Turning vanes mounted below and in front
157 of the wavemakers direct the current across the tank. These turning vanes
158 incorporate porous screens to provide flow conditioning and prevent debris
159 ingress to the plenum chamber [23]. This facility was selected due to the
160 large test area required for array testing.

161 In order to create an approximately uniform current across the test area
162 of the circular tank, the impeller units on either side of the required current

direction (i.e. both the upstream and downstream) are utilised. These are driven at varying speeds to produce the required current corresponding to the desired test velocity. This results in an ‘hour-glass’ shaped flow profile in the xy plane [24]. Previous measurements in the tank have shown the flow to be highly symmetrical about the stream-wise (x) axis [25]. However, in the streamwise direction there is some variation in both the mean and turbulent flow parameters. The velocity varies approximately linearly with depth but has a very shallow gradient compared with measurement at full scale sites [26].

3.2. Turbine Models

The small scale model utilised here is shown in Figures 1(bottom) and 2. The model has three 300mm wide (L) and 95mm chord length blades mounted on a planetary gear system. The distance from the primary shaft to the centre of rotation of each blade is 164mm. The cross sectional height of the turbine (D) is 200mm giving a ‘swept area’ (A) of 0.06 m². Note that this cross sectional area is not entirely swept by the blades due to the change of angle through the rotation, but since the design prohibits mounting another device within this cross sectional area the adopted definition was deemed the most appropriate. Ground force and Pelton effect plates, which act to increase the flow rate through the swept area, were added during early testing in order to increase rotational velocity [4]. Power take off is provided by a 2.5 kSt oil-filled dash-pot connected to the primary shaft by a 2:1 geared pulley and the angular velocity (ω) is measured via a 24 tabbed disk mounted on the primary shaft which passes through a Hall effect sensor. Part of the previous work focused on finding the gear ratio and damper which produced

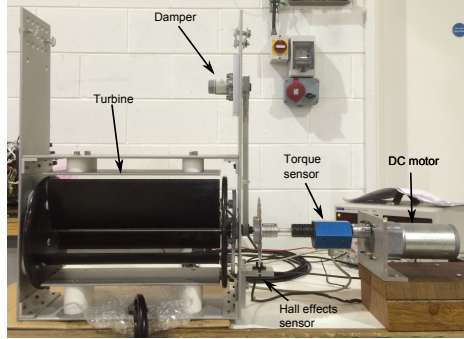


Figure 2: Model used in testing attached to torque calibration rig.

the highest power coefficient (c_p) [5].

The scale models utilised in these tests were by necessity relatively inexpensive to allow a relatively large number to be constructed and as such, there was some variation in angular friction from one turbine to the next. This is detailed further in Section 4.1. Therefore, it was necessary to calibrate the torque for each individual turbine and its damper for a range of rotational speeds. The rig for calibrating this torque curve is shown in Figure 2. It features a 2 Nm rotary torque transducer attached to the primary shaft and the system is driven by 27 W DC motor. For each turbine a measurement was taken every 2 V from 4 V to 24 V which provided a range of rotational speeds up to approximately 140 rpm. At each setting the rotational velocity (ω) and torque (τ) were collected via a National Instruments data acquisition system and recorded via Labview.

In order to mount the turbines in the tank, an adaptable frame design was developed that would allow for relatively quick changes between array configurations. Ideally the turbines would have occupied a greater percentage of the channel depth increasing the global blockage ratio. However, with the

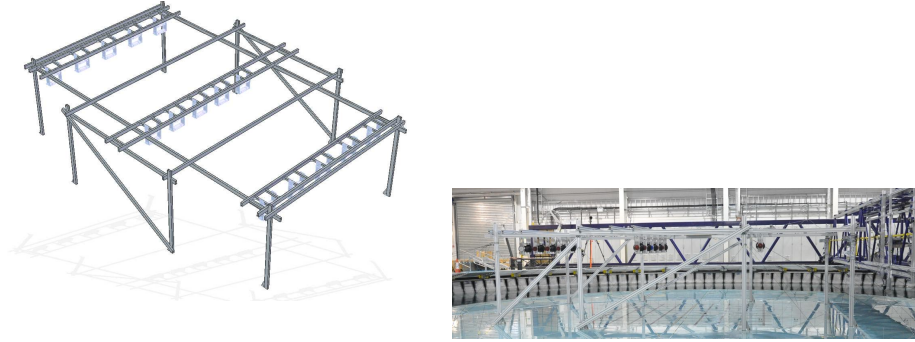


Figure 3: The frame for mounting the turbines, which was designed for high stiffness and for ease of reconfiguring turbine locations.

205 working depth of FloWave being 1.9 m this was not possible. The turbines
 206 were mounted close to the free surface as this would provide realistic blockage
 207 effects at one boundary as per the design specification [6]. Figure 3 shows
 208 the frame which was constructed from 45×90 mm cross section aluminium
 209 extrusion and Figures 5 and 6 highlight its location in the tank. In order to
 210 increase the rigidity of the frame, guy lines were tied to the tank floor from
 211 each of the vertical poles. In order to track any vibration of the frame and also
 212 the position of the turbines, a Qualisys tracking system was employed. This
 213 showed that under load the maximum movement in the frame was < 4 mm.

214 3.3. Array Layouts

215 Five different array layouts were tested in order to assess the effect of:
 216 lateral separation, stream-wise separation and in-line and staggered rows of
 217 turbines. To this end a base-case array layout was selected. Each of the other
 218 arrays vary one parameter from this base-case. The spacing are relative to
 219 the turbine dimensions where D is the cross flow height (equal to 200mm)
 220 and L is the cross-stream width (equal to 300mm).

Table 2: Overview of the array layout edge to edge spacings used in the tests. Bracketed numbers indicate the number of devices in each row.

Layout code	Staggered /In-line	x spacing	y spacing
Baseline	Staggered (4-5-4)	$14D$	$2L$
A	Staggered (4-5-4)	$10D$	$2L$
B	Staggered (4-5-4)	$14D$	$1.5L$
C	In-line (5-5-5)	$14D$	$2L$
D	In-line (5-5-5)	$14D$	$1.5L$

Each of the arrays featured three rows of turbines. All of these configurations included five turbines in the middle row. The staggered layouts had four turbines in the front and back with these spaced at the mid points in the transverse (y) between the middle row turbine locations. For the in-line arrays the turbines were mounted in the same y locations in each of the three rows, each containing five devices. The staggered arrays featured 13 turbines and the in-line 15 devices to accommodate this. Table 2 provides an overview of the array configurations which were investigated.

3.4. Measurement strategy

In addition to the rotational velocity of each turbine, the flow velocity within each array was investigated. In order to do this a Nortek Vectrino was utilised to measure the flow velocities. This instrument is capable of measuring at 100 Hz resolving the velocity into three Cartesian components. The Vectrino was mounted to the tank's instrumentation gantry on an adjustable frame, allowing it to translate in the x , y and z directions. As with any

236 acoustic sensor, measurements are subject to uncertainty due to noise. This
 237 Doppler noise is generally agreed to be zero mean, thus mean velocities are
 238 computed over a large number of samples (6000) to reduce the uncertainty.
 239 This noise will bias the turbulence intensity value high but this is corrected
 240 for by measuring the variance due to noise using the method described by
 241 Richard *et al.* [27].

242 To maximise the extent of velocity information from throughout the array,
 243 symmetry about the x axis was assumed, based on research that showed the
 244 undisturbed tank flow to be symmetrical [25] and that the frame and turbine
 245 array layouts were also symmetrical. All measurements were taken at a
 246 fixed depth at the midpoint of the turbine swept area. The co-ordinates
 247 for measurements are given in terms of their (x,y) position in mm from the
 248 centre point of the tank, where x is positive upstream of the centre.

249 For each array, one measurement (u_0) was taken significantly far upstream
 250 as to not be affected by the array as a reference. From there, one measure-
 251 ment was taken $2D$ upstream of each turbine on the $y \leq 0$ side of the array,
 252 this is referred to as the u_{in} measurement. In addition the development of
 253 the flow along the x axis is measured at $y = 0$ and at $y_{spacing}/2$. These were
 254 taken every $2D$ downstream (or as close as possible where the horizontal
 255 frame beams were obstructing access) from the first row to the last row of
 256 turbines. The positions of the array relative to the stream-wise direction of
 257 the tank were varied to minimise effects of the support struts on the flow.

258 Tests were carried out at the nominal, scaled current speed of 1.2 ms^{-1} ,
 259 although higher speeds were used on occasion to ensure all turbines cut-in,
 260 before being reduced to 1.2 ms^{-1} again for testing.

Each velocity vector is the result of one minutes measurement. This magnitude has previously been shown to be a statistically stationary period [26] and a mean value for each vector (e.g. \bar{u}) is reported. In addition to this, other metrics are used to give more information about the behaviour of the flow: the mean stream-wise velocity deficit (Δu), the turbulence intensity for each vector (i.e., I_u), the heading (θ), and the pitch (ψ) which are defined in the following equations:

$$\Delta u = 100 \cdot \left(1 - \frac{\bar{u}}{u_0}\right) \quad (1)$$

$$I_u = \frac{\sqrt{\sigma_u}}{\bar{u}} \quad (2)$$

$$\theta = \tan^{-1} \left(\frac{\bar{v}}{\bar{u}} \right) \quad (3)$$

$$\psi = \tan^{-1} \left(\frac{\bar{w}}{\bar{u}} \right) \quad (4)$$

3.4.1. Power

In order to compare the different arrays an appropriate metric must be defined. For the individual turbines the power extracted is given in Equation 5, where ω is the angular speed (in rad/s) and τ the torque of the turbine at that angular velocity calculated via the calibration curve detailed in section 4.1. The local power available in the flow (i.e. available to a specific device) is defined via Equation 6, where ρ is the fluid density and A the swept area of the turbine.

$$P_{turbine} = \omega\tau \quad (5)$$

$$P_{available} = 0.5\rho Au_{in}^3 \quad (6)$$

276 This allows the calculation of the power coefficient of the turbines, defined
277 via Equation 7:

$$c_p = \frac{P_{turbine}}{P_{available}} \quad (7)$$

278 Note that the central goal of this study is to maximise power output.
279 Thus, in order to compare the power captured by each of the array layouts,
280 three power metrics are used: P_{total} i.e. the sum of the mean power from each
281 turbine, P_{mean} the mean output from each individual turbine and finally $\frac{P_{total}}{m^2}$
282 the power per square meter of the array based on the total xy ‘footprint’ area
283 of the array configuration.

284 For tidal and wind turbines the power is often expressed as a function
285 of the Tip Speed Ratio which is the ratio of the velocity at the blade tip to
286 the velocity of the inflow fluid. As the MRL turbine tip speed is difficult to
287 define, here the Blade Speed Ratio (BSR) is used as an equivalent. BSR as
288 defined in [5] as:

$$BSR = \frac{\omega R}{u_{in}} \quad (8)$$

289 where ω is the angular velocity in rad/s and R is the radius to the axis of
290 blade rotation.

291 3.5. *Scaling and Blockage*

292 As there is no prototype scale device against which to scale the MRL
293 turbine, the depth and flow speeds of a typical tidal site of 50 m and 3 ms^{-1}

are considered respectively. These values do not represent estuary conditions, but given the depth of the test tank relative to the model turbine, this was deemed appropriate for this test, where the tank depth is significantly greater than the turbine diameter.

The two main scaling factors in tidal arrays are the Reynolds number, a ratio of the momentum to viscous forces, and the Froude number, a ratio of the inertia to the gravitational effects on the flow. These ratios are defined in equations 9 and 10 where ρ is the density, l is a characteristic length and g is the gravitational field strength [17]. For the same fluid and gravitational forces these two dimensionless quantities can not be equally scaled. However, flow conditions are required to be within the same regimes, i.e., fully developed turbulence and sub-critical [28].

$$Re = \frac{\rho ul}{\mu} \quad (9)$$

$$Fr = \frac{u}{\sqrt{gl}} \quad (10)$$

If l is taken to be the channel depth and g is taken to be constant at 9.81 ms^{-1} , the Re and Fr numbers for this test and for the nominal site are given in Table 3. These numbers are in the range of those in similar work [17].

Whilst some authors have envisaged that Froude number has minor influence in power and thrust (both increase about 3% according to [29]), the discrepancy between Reynolds numbers between prototypes and full scale devices has large effects in the performance of a tidal turbine. In Mycek *et al.* [30], Reynolds numbers from 1.4×10^5 to 4.2×10^5 were used in the

Table 3: Comparison of scaling parameters

	Re	Fr
FloWave	2.4×10^6	0.32
Full Scale	1.3×10^8	0.09

315 experimental campaign. It was demonstrated that the c_p of a turbine can in-
 316 crease by about 10% when working at larger flow velocities and hence larger
 317 Reynolds numbers. This increase is somehow to be expected, Mason-Jones
 318 *et al.* [31] suggested that in order to reach Reynolds independence, Reynolds
 319 numbers higher than 3×10^5 should be contemplated in small scale test cam-
 320 paigns. However, this insensitivity of Reynolds number could be dependent
 321 on the aerofoil shape but according to the authors knowledge there is no ev-
 322 idence to prove it. As it has been envisaged by Selig *et al.* [32], wind tunnel
 323 tests have demonstrated that the magnitude of lift on thick aerofoils can be
 324 increased slightly when increasing Reynolds numbers from 1×10^5 to 5×10^5 .
 325 However, the effects on drag will be severely, in some cases an increase of
 326 50 - 80% was observed at angles of attack between 0 to 10 degrees. This
 327 proportion depends on the type of aerofoil shape, in this case the S822 was
 328 taken as an example. Wind tunnel tests studies will need to be considered
 329 in the next development stages of the MRL turbine due to the constant and
 330 different changes in angle of attack related to each of the blades.

331 As previously stated the blockage for this test is relatively low compared
 332 with early tests of this device and other arrays. The swept area of the
 333 staggered arrays are $9 \times A$ which is: $0.2 \times 0.3 \times 9 = 0.54 \text{ m}^2$. The tank area
 334 at the mid point as $25 \times 1.93 = 48.25 \text{ m}^2$. This leads to a global blockage

ratio of 0.010 for the staggered arrays and of 0.005 for the in-line arrays with a swept area of $5A$.

4. Results

4.1. Turbine Calibration

The calibration results from each of the turbines with dampers installed are presented in Figure 4. The dashpot's resistance changes with temperature which is related to ω hysteretically. Thus, the calibration was repeated in ascending and descending ω to capture this effect. As can be seen, there is a spread of values with a maximum difference at the highest voltage used of 0.26 Nm indicating a significant degree of variation in damping between devices. It can be noticed that the turbine 3A, which used an older damper of the same specification, showed the lowest resistance, indicating that the performance of these devices in this installation were decreasing over time or with use.

Multiple types were trialled to this data (using the downward calibration curve as all turbine measurements were taken at established speeds). The power law gave the highest goodness of fit values thus this fit type was adopted. The form of this curve is given in Equation 11, where a and b are constants defined individually for each turbine.

$$\tau = a \cdot \omega^b \quad (11)$$

4.2. Base-Case

As a large quantity of data was collected for each array, greater detail is provided for the base-case layout, which will provide values which can be

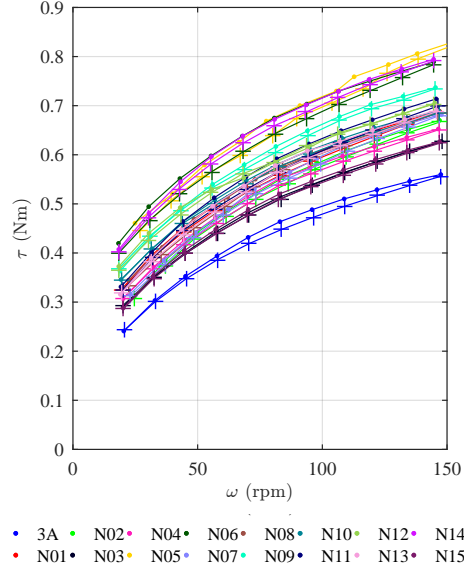


Figure 4: Results of individual turbine torque calibrations. Dots mark the curve for increasing ω and crosses for decreasing.

357 contrasted with other layouts.

358 Figure 6 shows the positions of the turbines, the positions of the vertical
 359 pillars, the velocity measurements taken during the test, as well as the ve-
 360 locity measurements in the tank with no devices installed taken from Noble
 361 *et al.* [25]. This gives an illustration of where measurements were taken and
 362 the effect of the turbines on the flow velocity. These measurement locations
 363 do not capture the effects of the vertical support poles of the frame on the
 364 flow during the testing, which were observed, visually, to be significant.

365 4.2.1. Velocity deficit and turbulence intensity

366 Focusing on the two sets of stream-wise velocity measurements, Figure 7
 367 shows the evolution of the flow through the turbines. As can be seen there is

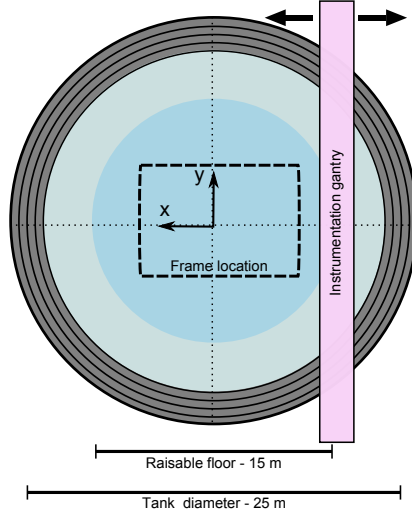


Figure 5: Illustration of test area, detailed in Figure 6, in dotted line and its position within the FloWave tank. Co-ordinate system is given from the tank centre.

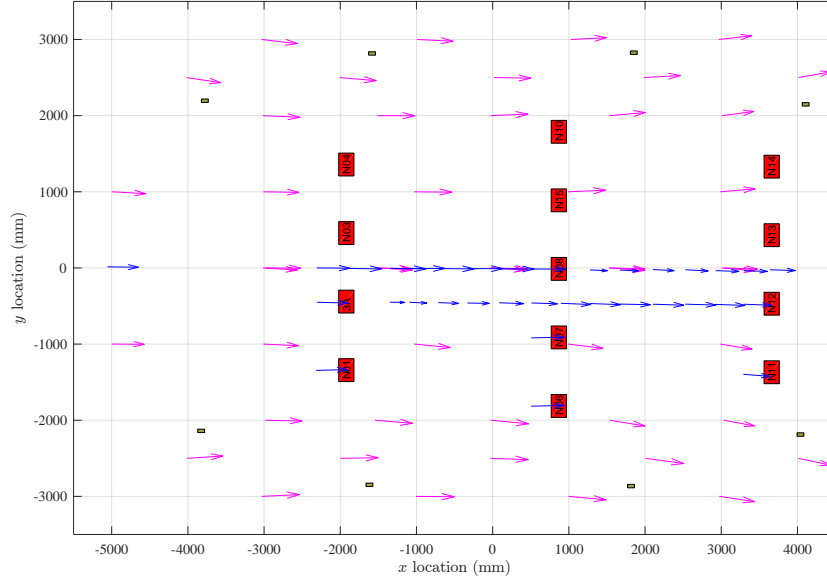


Figure 6: Quiver plot for the base-case array. Blue arrows represent in-situ velocity measurements, the pink arrows represent the ‘natural’ flow in the tank were there no obstructions. The large red rectangles represent the turbines and the small grey ones the vertical frame poles.

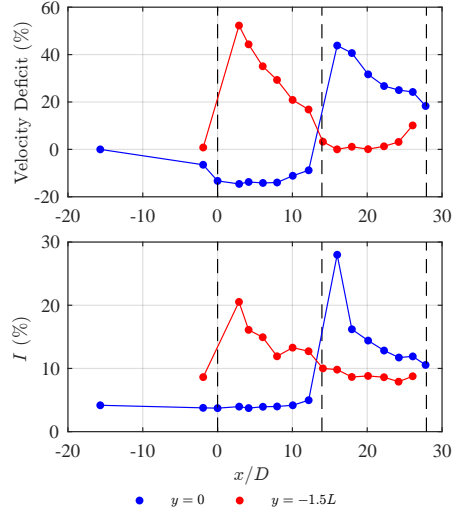


Figure 7: Velocity deficit and turbulence intensity of flow as it propagates through the base-case array. The dashed lines indicate the location of the turbine rows. Flow moving from left to right.

368 an acceleration from the upstream measurement point due to the tank flow
 369 geometry then an acceleration through at the centreline through the first row
 370 of turbines. There is a large decrease in velocity of 52% as the flow passes
 371 through a turbine with a similar decrease at $y = -1.5L$ over the turbine in
 372 the middle row of 54%. There is a corresponding jump in turbulence intensity
 373 at each row of 12% and then 26%. It is interesting to note that, although the
 374 velocity deficits are approximately equal, in each case the downstream jump
 375 in I is significantly greater. Downstream of the turbines, the velocity and I
 376 start to recover towards their upstream values.

377 4.2.2. Velocity direction

378 A phenomenon which became apparent during testing was a standing
 379 surface wave downstream of the first row (Figure 8). This effect had been

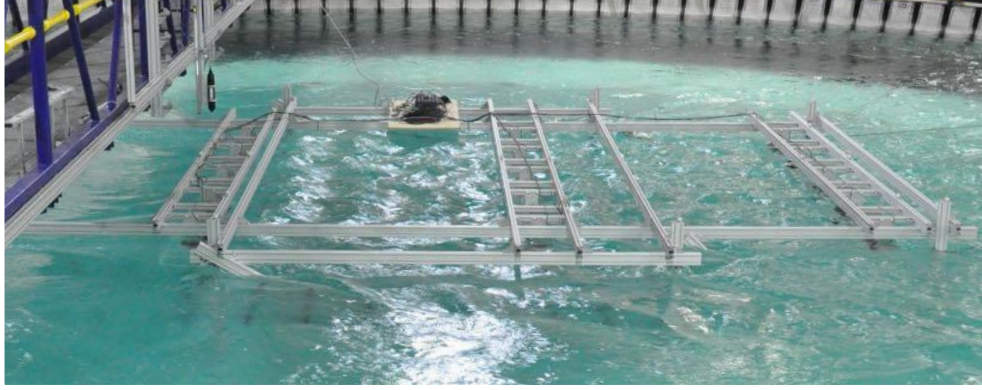


Figure 8: Evidence of ‘standing wave’ effects in wake. Flow moving from left to right.

380 previously noted in other experiments and predicted by CFD [17, 4].

381 The pitch and heading angles as the flow propagates through the rows of
 382 turbines are presented in Figure 9. The heading angles are relatively small
 383 ($< 5^\circ$) throughout. In the majority of cases, there is a $\sim 4^\circ$ shift of the flow
 384 to the left each time the flow passes through a row of turbine. This was
 385 only observed for the centre-line measurements in the base-case array. The
 386 measurements of the pitch angle of the flow are an order of magnitude greater
 387 than those of the heading. The measurement resolution is not high enough
 388 to capture properly the sinusoidal pattern visually observed. However, there
 389 is evidence of this effect between the first and second turbine rows. Each
 390 time the flow passes the turbine there is an upward shift in the pitch angle,
 391 which corresponds to the rotational direction of the turbine. The flow in the
 392 main has a small negative pitch angle, i.e. a downward trajectory.

393 *4.3. Turbine Performance*

394 The mean and standard deviation of individual turbine ω values for the
 395 base-case array are given in Figure 10. A large variation in values which

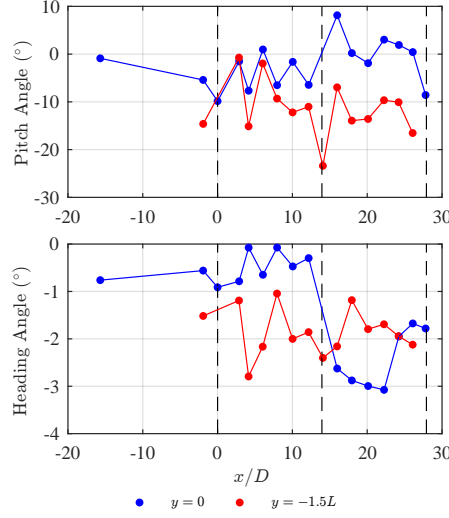


Figure 9: Results of velocity direction through the base-case array. Flow moving from left to right.

is due to the variability of both inflow velocity through the array and the damping of the individual turbines can be seen.

In order to examine the variation of damping between devices, the angular velocity is converted to a c_p value through equations 5, 6, 7 and 11. Limiting the results to those for which the inflow is directly measured (rather than inferred through the assumption of a symmetrical array) the c_p for the Blade Speed Ratio (BSR) is shown in Figure 11. This analysis uses Array A as there was an additional inflow measurement available.

It can be seen that the c_p values for the turbines in the front and middle rows are approximately linear on a positive gradient, suggesting power capture increases as turbine damping decreases. However, the two back row values do not conform to this trend. These results suggest that the downstream turbines with inflows from the wakes of the upstream turbines are

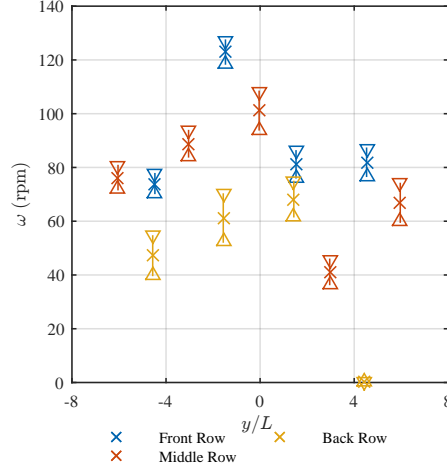


Figure 10: Base-case array mean and standard deviations of ω .

less predictable than those upstream.

The $\overline{u_{in}}$, $\overline{\omega}$ and \overline{P} for each turbine in the base-case array are presented in Figure 12. It is reiterated that the $\overline{u_{in}}$ measurements are only measured for half of each array layout and the $y > 0$ values are inferred by assuming symmetry about the x axis. One aspect that is evident is the lack of symmetry in the measured ω and P values. In the top plot it can be seen that the middle row has the highest inflow velocities due to the blockage of the flow through the upstream turbine row. However, this higher u_{in} does not correspond to higher rotational velocities in the middle plot. As the turbulence intensity is also constant into both rows it is inferred that it is the vertical component of the velocity (i.e. the pitch of the flow as per Figure 9) that is affecting the reduction in ω in the middle row devices. The power is highly variable between devices in the two front rows, with the back row presenting the lowest variation and generally lowest response.

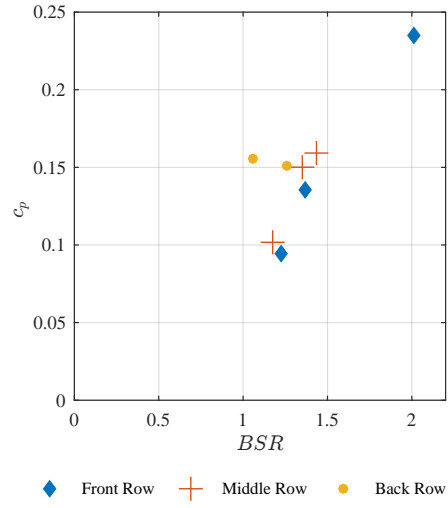


Figure 11: c_p variation between turbines for array A.

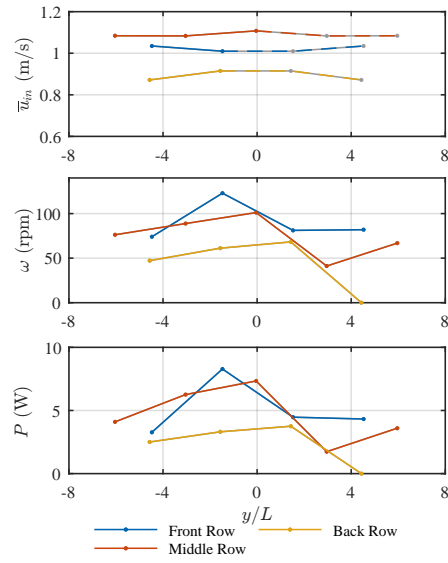


Figure 12: $\overline{u_{in}}$, $\overline{\omega}$ and \overline{P} for each turbine in the base-case array.

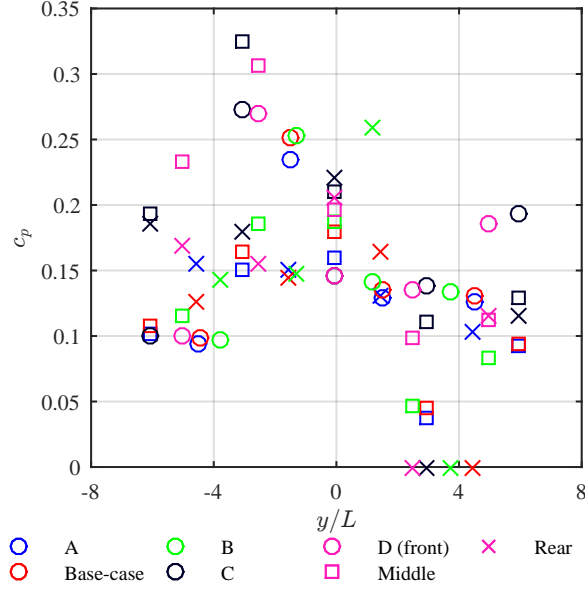


Figure 13: All c_p values across the 5 arrays. Circles mark the front row, squares the middle and crosses the rear row, with colours indicating the array layout.

4.4. Inter Array Comparisons

The $\overline{u_{in}}$, $\overline{\omega}$ and \overline{P} values for each turbine for the four additional array layouts are given in Figures 14, 15, 16 and 17, with the base-case included in grey for comparison.

For the decreased stream-wise separation (Figure 14) the trends are very similar to those in the base-case array, with highest flow velocities being into the middle row of turbines due to acceleration between the first row turbines and similar ω values. In the decreased lateral spacing case (Figure 15) the velocity into the second row is very similar to the front row, suggesting that at this spacing the first turbine row as a whole has a blockage ratio that is causing more flow to divert round the sides of the array. The reason of this diversion is because the flow has reached its maximum choking capacity

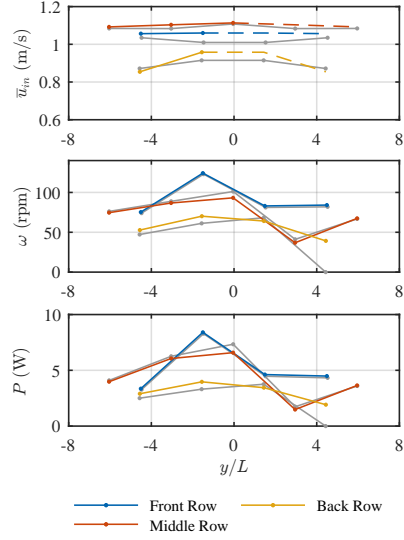


Figure 14: $\overline{u_{in}}$, $\overline{\omega}$ and \overline{P} for array layout A, with base-case results in grey.

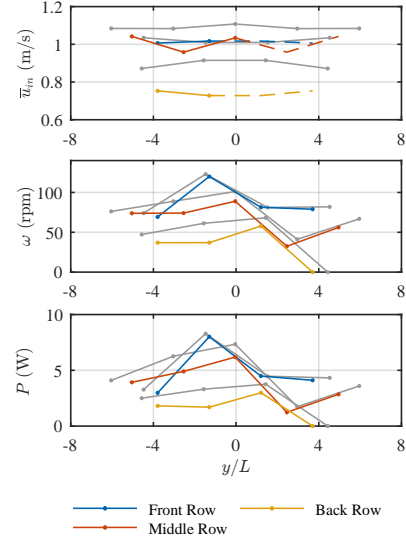


Figure 15: $\overline{u_{in}}$, $\overline{\omega}$ and \overline{P} for array layout B, with base-case results in grey.

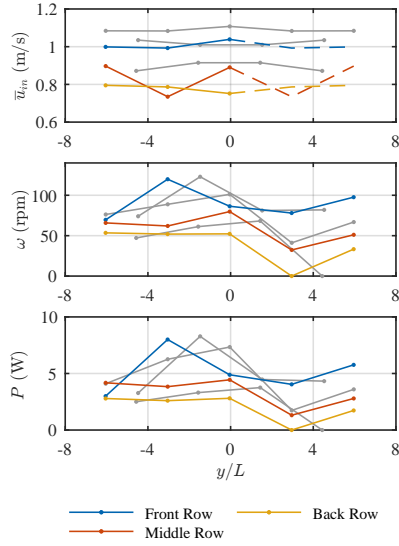


Figure 16: $\overline{u_{in}}$, $\overline{\omega}$ and \overline{P} for array layout C, with base-case results in grey.

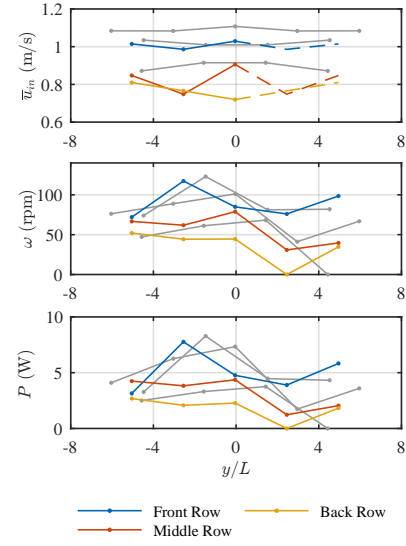


Figure 17: $\overline{u_{in}}$, $\overline{\omega}$ and \overline{P} for array layout D, with base-case results in grey.

435 which as defined by Nishino and Willden [15], is the reduced ow through an
436 entire array. For all three of the staggered arrays there is little asymmetry of
437 P and ω results around the stream-wise axis in any of the rows. The trends
438 in these metrics are, however, consistent between the three staggered array
439 layouts.

440 In the two in-line arrays (Figures 16 and 17), u_{in} is highest in the front
441 row as would be expected. However, there is evidence of the wake from the
442 upstream posts affecting the inflow to the middle row at the second turbine
443 from each edge in both array spacings, leading to those turbines having lower
444 u_{in} than the back row. This is not directly reflected in the ω and P results
445 which decrease row by row.

446 This asymmetry of power and angular velocity across the 5 arrays (seen in
447 Figures 14 to 17), may in part be due to the direction of the flow in the tank
448 which forms an hour glass shape [26]. Although through the majority of the
449 test area the flow is uniform, at the edges a combination of this inward flow
450 and the wake of the vertical poles may cause flow velocities from different
451 directions to affect the turbines. However, the effect is relatively constant
452 across the arrays suggesting that power comparisons are valid.

453 It has been observed in the literature that there are some effects on the
454 power captured depending on the direction of the flow. However, Figure
455 9 shows that the heading angles in these tests are less than 4 degrees and
456 therefore it was envisaged that such small angles will not have a significant
457 impact in the power calculations. This supposition was due to the research
458 presented by Galloway *et al.* [33] who showed that power reductions only
459 become apparent with heading angles above 7.5 degrees. Also, the turbulence

intensities at the outer turbines are greater than that at the u_{in} locations for
 the inner turbines, with range of values increasing from 4 - 14% to 14 - 25%.
 Figure 18 shows how the velocity deficit and I values vary in the in-line
 Array C. For the first and second turbine row there is a Δu of 51% and 45%
 respectively, with a recovery to within 13% of the upstream value by $12D$.
 The sharp peak in I midway between the front and centre row exists at both
 spacing but it is not clear what the driving factor is. It may be a mixing point
 for the turbine wakes, but the spatial resolution of velocity measurements is
 insufficient to analyse.

In order to assess which array is the best, three power related metrics are
 employed. The results of power for each configuration are given in Table 4.
 In terms of total power, four of the five arrays show similar values with the
 narrow staggered Array B being the lowest and the base-case the highest.
 The total power per device is dominated by the two 0.6m spaced staggered
 arrays, which both have thirteen devices, two less than the in-line arrays. In
 terms of power for a given footprint-area, it is Array A (decreased stream-
 wise spacing) that gives the best results.

Figure 13 shows all the c_p values across the five array configurations.
 The highest value is 0.32 which is for the middle row of Array C. The mean
 value, discounting any non-rotating devices, is 0.15. There is evidence of
 the asymmetry in the arrays with the values on the left ($y/L < 0$) being
 significantly higher than those on the right, which is relatively consistent
 across the array layouts.

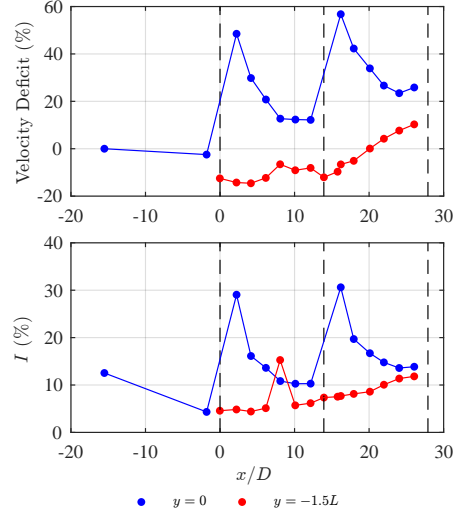


Figure 18: In-line array ‘C’ showing the Velocity deficit and I across two sets of turbines.

Table 4: Power parameters from each array layout.

	Array				
	Base-case	A	B	C	D
Total P (W)	55.4	54.8	47.0	54.8	52.0
P per Device (W)	4.3	4.2	3.6	3.7	3.5
P per xy	2.8	3.8	2.8	2.7	3.1
area (W/m ²)					

483 5. Discussion

484 The three power metrics show that Array A has the highest power per
 485 footprint area and the base-case the highest total power. Comparing the
 486 trends from the base-case with similar trends in the CFD work [7, 8]: the
 487 decreasing lateral separation had the opposite effect on power in the CFD
 488 study compared to the current experiments. It should be noted that in
 489 the experimental work these separations are $2L$ and $1.5L$ (due to practical
 490 limits of the tank) whereas in the CFD these are $2L$ and $4L$. Malki *et al.*
 491 [34] suggests that a lateral spacing of $1D$ represents a critical ratio after
 492 which decreased lateral separation decreased the bypass flow. This reverse of
 493 trend between experimental and CFD results is likely due to the experiments
 494 operating in the region of this the critical array ‘choking’ capacity. Only
 495 two lateral separations were tested in this work and thus a useful follow
 496 up study would focus on finding the exact point of lateral separation for
 497 maximum downstream turbine power. Likewise the downstream separation
 498 will allow mixing to occur (decreasing I and increasing u at the inflow to
 499 downstream devices) but also requires a greater xy area and there will likely
 500 be a maximum value of P/A in this trade off.

501 The c_p values recorded are similar to those in Ordonez *et al.* [5] but
 502 lower than earlier studies [4] and lower than for other small-scale turbine
 503 experiments [35] which both produced maximum values of $c_p > 0.45$. It
 504 should be noted that the MRL turbines were designed for high blockage
 505 ratio flows and thus the c_p results presented were expected to be lower than
 506 these high blockage tests. If a suitable facility could be found, a repeat test in
 507 shallow water, where the turbines could be mounted to the floor to avoid the

508 effects of structural struts on the flow would be of benefit. In addition, work
509 by Salter and Taylor [36] and Nishino *et al.* [15] has suggested that very high
510 global blockage ratios would increase c_p and allow the Lanchester-Betz limit
511 to be exceeded. This is due to the tidal channel being more analogous to a
512 duct than unbounded flow for which the limit was defined. This would require
513 larger turbine models or a shallower tank to effectively test this hypothesis,
514 which remains a key query for the industry.

515 An interesting wake effect was the standing wave at the free surface behind
516 the first row of turbines. This effect was also noted in the results of [17], who
517 speculated it could be due to critical bypass flow. However, with the Froude
518 numbers in this experiment of 0.32 being significantly below the critical value
519 of 1, it is far more likely the effect is due to vertical mixing and head loss
520 across as the flow travels through the turbine. This varying flow direction
521 will change the effective angle of attack of the blades in downstream devices.
522 There is likely to be a ‘sweet-spot’ within the wavelength of the standing
523 wave that will improve efficiency of downstream devices. This will be at the
524 angle relative to the blade acting primarily in lift (rather than drag) where
525 the flow direction has the effective angle of attack of highest lift coefficient.
526 It was also noted that the pitch angle had a small negative (downward)
527 velocity throughout the measurements. This may in part be due to a small
528 misalignment of the ADV in this plane.

529 A key source of uncertainty in this experimental work was the asymmetry
530 in the turbines’ in-flow velocity. A previous study validated the symmetry of
531 the flow in facility and the turbines and the frame were mounted symmetri-
532 cally about the centre line of the tank. Due to this the inflow to individual

533 turbines was only conducted for half the devices, in order to maximise the
534 number of arrays that could be trialled in the available test time. The results
535 presented show that there are changes in flow heading as it passes through
536 the arrays. While Ordonez et al. [5] observed evidence of asymmetry in the
537 wake, no measurements were made of the transverse velocity components.
538 Thus, no direct comparison can be made with the present tests and the
539 measured transverse flow velocities. It is recommended for future tests that
540 inflow measurements are taken for all devices. In addition advancing the
541 models to a higher degree of sophistication including active torque or speed
542 control could reduce variation of results between devices.

543 In addition to this, the wake from the support poles played a large role
544 in the results. Different turbine array layouts were affected differently due
545 to different turbine positions relative to these poles. While this increases the
546 uncertainty of these results, it is also a reminder of the sensitivity of machine
547 performance to likely complex local flows in a real field setting.

548 In summary there are three proposed optimising spacings for this type of
549 turbine in arrays:

- 550 1. A stream-wise spacing to maximise P_{total}/A of the order of multiple
551 rotor diameters;
- 552 2. A lateral spacing to maximise bypass flow, i.e., the array ‘choking’
553 capacity;
- 554 3. A refinement of the stream-wise spacing of the order of a single rotor
555 diameter, to find the optimum performance within the standing wave
556 wavelength.

557 It is still a point of debate as to which metric is best for comparing arrays.

558 Power per xy area is one logical choice but this is only worthwhile if the area
559 constraint is likely to be the dominant parameter in the array design. This
560 subject would require a site optimisation tool and is likely project specific.

561 As this work represents one of the largest array testing projects to use
562 rotating models at this scale, there is significant scope for future work, beyond
563 what has already been discussed in this section. An expansion to compare
564 different turbine types such as conventional three-bladed HATs would inform
565 differences in array spacings for different designs. It is obvious from the
566 results presented that flows through arrays are complex and it is best to
567 measure at as high a spatial resolution as resources allow. Finally, for many
568 tidal sites the direction of flow varies significantly [10]. Hence a test of array
569 sensitivity to off angle flow is a key metric to predict total power over a full
570 tidal cycle.

571 As the first commercial arrays of devices are shortly to become a reality,
572 the increased knowledge of flow interaction and array layout optimisation
573 represent essential knowledge. However, with many key question still asso-
574 ciated with a high level of uncertainty further work is needed to ensure the
575 successful progression of the industry.

576 6. Conclusions

577 Comparing the power extracted for each trend in the arrays the following
578 conclusions can be drawn:

- 579 • Power extraction changes the flow through the arrays, with the power
580 per turbine varying by up to 19% in the arrays presented. Thus posi-
581 tioning turbines is important to maximise power output as predicted.

- 582 • Increasing streamwise spacing increases the total power captured in the
583 staggered arrays (base-case and A). This is as predicted by [16] who
584 suggest that downstream rows will be less effected by the performance
585 of upstream rows.
- 586 • Staggering rows generally improves the power per device as predicted
587 by [16].
- 588 • Decreasing lateral spacing can increase or decrease power output as
589 there is an optimal local blockage to maximise power output [15]. The
590 results here show a decrease in power output for both staggered and
591 in-line arrays suggesting that the spacing in the narrow arrangements
592 (arrays B and D) are at a spacing less than this critical array ‘choking’
593 capacity.

594 **Acknowledgements**

595 The authors would like to thank Nortek UK for the loan of the Vectrino
596 Profiler for use in these experiments. We would also like to thank the fol-
597 lowing staff at The University of Exeter who worked so hard to support the
598 model construction: Siobhan Kelley, Jordana Broom & Steve Redshaw. The
599 authors would also like to acknowledge the EPSRC for funding this work
600 under grant number: EP/J010138/1.

601 **References**

- 602 [1] C. Legrand, Assessment of Tidal Energy Resource, Tech. rep., Black and
603 Veatch, EMEC (2009).

- 604 [2] Carbon Trust, UK Tidal Current Resource and Economics Study, Tech.
605 Rep. July (2011).
- 606 [3] DECC, Digest of UK Energy Statistics: Chapter 5 Electricity (2015)
607 113–155doi:10.1227/01.NEU.0000028161.91504.4F.
- 608 [4] A. P. Janssen, M. R. Belmont, Initial research phase of MRL turbine.
609 Technical report, Technical Report No: MO 562L.
- 610 [5] S. O.-S. D. S. G. S. P. T. B. M. G. M. R. B. I. Moon, Experimental
611 Evaluation of the Wake Charecteristics of Cross Flow Turbine Arrays,
612 Ocean Engineering.
- 613 [6] M. G. Gebreslassie, G. R. Tabor, M. R. Belmont, CFD simulations
614 for investigating the wake states of a new class of tidal turbine, in:
615 International Conference on Renewable Energies and Power, 2012.
- 616 [7] M. G. Gebreslassie, G. R. Tabor, M. R. Belmont, Numerical simulation
617 of a new type of cross flow tidal turbine using OpenFOAM - Part I:
618 Calibration of energy extraction, Renewable Energy 50 (2013) 994–1004.
619 doi:10.1016/j.renene.2012.08.065.
- 620 [8] M. G. Gebreslassie, G. R. Tabor, M. R. Belmont, Numerical simula-
621 tion of a new type of cross flow tidal turbine using OpenFOAM - Part
622 II: Investigation of turbine-to-turbine interaction, Renewable Energy 50
623 (2013) 1005–1013. doi:10.1016/j.renene.2012.08.064.
- 624 [9] M. G. Gebreslassie, G. R. Tabor, M. R. Belmont, Investigation of the
625 performance of a staggered configuration of tidal turbines using CFD,

- Renewable Energy 80 (2015) 690–698. doi:10.1016/j.renene.2015.03.001.
- [10] B. G. Sellar, D. R. J. Sutherland, MD 3.8 - Tidal energy site characterisation at the fall of warness, EMEC, UK, techreport, available from: <http://redapt.eng.ed.ac.uk/> (2015).
- [11] T. H. E. Clark, Turbulence in Marine Environments (TiME): A framework for understanding turbulence and its effects on tidal devices., In review.
- [12] T. Stallard, R. Collings, T. Feng, J. Whelan, Interactions between tidal turbine wakes: Experimental study of a group of 3-bladed rotors, Philosophical Transactions of the Royal Society of London: A 371 (1985) (2013) 1471–2962.
- [13] S. G. Parkinson, T. Stallard, M. Thomson, a. Wickham, R. Willden, Comparison of scale model wake data with an energy yield analysis tool for tidal turbine farms, 4th International Conference on Ocean Energy (2012) 2–6.
- [14] T. Daly, L. Myers, A. Bahaj, Numerical analysis of the acceleration and wake effects resulting from changes in tidal turbine array position in a channel (2011) 1–9.
- [15] T. Nishino, R. H. J. Willden, The efficiency of an array of tidal turbines partially blocking a wide channel, Journal of Fluid Mechanics 708 (2012) 596–606. doi:10.1017/jfm.2012.349.

- 648 [16] S. Draper, T. Nishino, Centred and staggered arrangements of tidal
649 turbines, *Journal of Fluid Mechanics* 739 (2014) 72–93. doi:10.1017/
650 jfm.2013.593.
- 651 [17] S. Draper, T. Stallard, P. Stansby, S. Way, T. Adcock, Laboratory scale
652 experiments and preliminary modelling to investigate basin scale tidal
653 stream energy extraction, in: 10th European Wave and Tidal Energy
654 Conf., Aalborg, Denmark, 2013.
- 655 [18] J. G. Leishman, Challenges in modelling the unsteady aerodynamics of
656 wind turbines, *Wind Energy* 5 (2-3) (2002) 85–132. doi:10.1002/we.
657 62.
- 658 [19] R. Vennell, S. W. Funke, S. Draper, C. Stevens, T. Divett, Designing
659 large arrays of tidal turbines: A synthesis and review, *Renewable and*
660 *Sustainable Energy Reviews* 41 (2015) 454–472. doi:10.1016/j.rser.
661 2014.08.022.
- 662 [20] L. E. Myers, A. S. Bahaj, An experimental investigation simulating
663 flow effects in first generation marine current energy converter arrays,
664 *Renewable Energy* 37 (1) (2012) 28–36. doi:10.1016/j.renene.2011.
665 03.043.
- 666 [21] S. C. Cooke, R. H. J. Willden, B. W. Byrne, T. Stallard, A. Olczak, Ex-
667 perimental Investigation of Thrust and Power on a Partial Fence Array
668 of Tidal Turbines, in: 11th European Wave and Tidal Energy Confer-
669 ence, Nantes, France, 2015, pp. 1–10.

- 670 [22] P. Mycek, B. Gaurier, G. Germain, G. Pinon, E. Rivoalen, Numerical
671 and experimental study of the interaction between two marine current
672 turbines, *International Journal of Marine Energy* 1 (2013) 70–83. [arXiv:](#)
673 [1310.4921](#), [doi:10.1016/j.ijome.2013.05.007](#).
- 674 [23] A. Robinson, D. Ingram, I. Bryden, T. Bruce, The effect of inlet de-
675 sign on the flow within a combined waves and current flumes, test tank
676 and basins, *Coastal Engineering* 95 (2015) 117–129. [doi:10.1016/j.](#)
677 [coastaleng.2014.10.004](#).
- 678 [24] A. Robinson, I. Bryden, D. Ingram, T. Bruce, The use of conditioned ax-
679 ial flow impellers to generate a current in test tanks, *Ocean Engineering*
680 75 (2014) 37–45. [doi:10.1016/j.oceaneng.2013.10.016](#).
- 681 [25] D. R. Noble, T. Davey, H. C. M. Smith, P. Kaklis, A. Robinson,
682 T. Bruce, Spatial variation in currents generated in the FloWave Ocean
683 Energy Research Facility, in: 11th European Wave and Tidal Energy
684 Conference, Nantes, France, 2015.
- 685 [26] D. R. J. Sutherland, D. R. Noble, J. Steynor, T. Davey, T. Bruce, Char-
686 acterisation of Current and Turbulence in the FloWave Ocean Energy
687 Research Facility, *Ocean Engineering* 139, 15 July 2017, Pages (2016)
688 103–115.
- 689 [27] J.-B. Richard, J. Thomson, B. Polagye, J. Bard, Method for identifica-
690 tion of Doppler noise levels in turbulent flow measurements dedicated to
691 tidal energy, *International Journal of Marine Energy* 3-4 (2013) 52–64.
692 [doi:10.1016/j.ijome.2013.11.005](#).

- 693 [28] A. Chadwick, J. Morfett, M. Borthwick, *Hydraulics in civil and envi-*
694 *ronmental engineering*, 4th Edition, 2004.
- 695 [29] S. C. M. Claudio A Consul, Richard H. J Willden, Blockage effects on the
696 hydrodynamic performance of a marine cross-flow turbine, *Philosophical*
697 *Transactions of the Royal Society* Adoi:10.1098/rsta.2012.0299.
- 698 [30] P. Myceka, B. Gaurierb, G. Germainb, G. Pinona, E. Rivoalena, Exper-
699 imental study of the turbulence intensity effects on marine current tur-
700 bines behaviour. Part I: One single turbine, *Renewable Energy* 66 (June)
701 (2014) 729–746.
- 702 [31] A. M.-J. D. O. C. M. T. O. C. B. P. P. R. G. I. O. S. T. R. Poole,
703 Non-dimensional scaling of tidal stream turbines, *Energy*.
- 704 [32] A. P. B. Michael S. Selig, James J. Guglielmo, P. Giguere, Summary of
705 low-speed airfoil data vol. 1, Tech. rep., Department of Aeronautical and
706 Astronautical Engineering, University of Illinois at Urbana-Champaign.
707 SOARTECH Publications. (1995).
- 708 [33] P. G. L. M. A. Bahaj, Experimental and numerical results of rotor power
709 and thrust of a tidal turbine operating at yaw and in waves, in: *World*
710 *Renewable Energy Congress - Marine and Ocean Technology*, Linkoping,
711 2011.
- 712 [34] R. Malki, I. Masters, A. J. Williams, T. Croft, Planning tidal stream
713 turbine array layouts using a coupled blade element momentum com-
714 putational fluid dynamics model, *Renewable Energy* 63 (2014) 46–54.
715 doi:10.1016/j.renene.2013.08.039.

- 716 [35] A. S. Bahaj, A. F. Molland, J. R. Chaplin, W. M. J. Batten, Power and
717 thrust measurements of marine current turbines under various hydrody-
718 namic flow conditions in a cavitation tunnel and a towing tank, Renew-
719 able Energy 32 (3) (2007) 407–426. doi:10.1016/j.renene.2006.01.
720 012.
- 721 [36] S. H. Salter, J. R. M. Taylor, Vertical-axis tidal-current generators and
722 the Pentland Firth, Proceedings of the Institution of Mechanical En-
723 gineers, Part A: Journal of Power and Energy 221 (2) (2007) 181–199.
724 doi:10.1243/09576509JPE295.